Iranian Journal of Astronomy and Astrophysics
Vol. 11, No. 3, Summer 2024, 231–243
©Available online at http://ijaa.du.ac.ir
DOI: 10.22128/ijaa.2025.814.1181
Online ISSN: 2383–403X

Iranian Journal of Astronomy and Astrophysics

Research Paper

The Study of AutoCorrelation Function on Lyman Alpha Forest of QSOs

Sara Rezaee Darestanee[1] · Reza Pazhouhesh*[2] · Alireza Aghaee[3]

[1] Department of Physics, Faculty of Sciences, University of Birjand, Birjand, Iran;
email: rezaee.s@birjand.ac.ir

[2] Department of Physics, Faculty of Sciences, University of Birjand, Birjand, Iran;
*email: rpazhouhesh@birjand.ac.ir

[3] Department of Physics, Faculty of Sciences, University of Sistan and Baluchestan, Zahedan, Iran;
email: aghaee@phys.usb.ac.ir

Received: 19 March 2024; **Accepted:** 09 January 2025; **Published:** 13 January 2025

Abstract. The Lyman Alpha (Lyα) forest is one of the most powerful cosmological tools for studying large-scale structures of the universe. The flux autocorrelation function for Lyα forest is used to study the clustering of structures. This paper uses the Lyα forest of 49 high-resolution, high signal-to-noise ($S/N > 20$) QSO spectra observed with VLT/UVES. The studied quasars have emission redshifts in the range of ($1.89 < zemi < 3.80$). The flux autocorrelation function is calculated for each sample, and then, the effect of metal absorption lines in the Lyα forest on the flux autocorrelation function is investigated. The results of the present study show that the effect of removing metal absorption lines is more visible in the transition to lower redshifts, where there are relatively fewer Lyα absorption lines. Moreover, the change in the flux autocorrelation function at different redshifts is investigated. The results indicate that the flux autocorrelation function at higher redshifts has a larger average value than that at lower redshifts.

Keywords: IGM: Large scale structure, Autocorrelation function, Quasar: Absorption systems, Lyman alpha forest

1 Introduction

Lyman alpha (Lyα) forest describes the $n = 1$ to $n = 2$ transition in the Lyα absorption spectrum of neutral hydrogen in the background quasistellar objects (QSOs). The exact nature of quasars was unknown for some time, but now it is clear that quasars are galaxies with extremely high luminosity because of supermassive black hole accretion [1].

As the universe expands, quasar light is redshifted on its path to observers. Neutral hydrogen in the intergalactic medium (IGM) absorbs the redshifted light at a specific wavelength of the Lyα transition. In 1965, Gunn and Peterson suggested that in a homogeneously gas-filled universe with expansion, an absorption trough blueward of the Lyα emission line can be found because of the absorption of the redshifted Lyα line [2]. In the same year, Bahcall and Salpeter suggested that discrete lines in the quasars' spectra may indicate the

* *Corresponding author*

absorption from intervening neutral hydrogen clouds in the line of sight [3]. In 1971, Lynds discovered these patterns of absorption, also known as the Lyα forest, in the spectra of a quasar [4].

After the discovery of the Lyα forest, several studies have revealed that the predominant pattern of this environment can be described as a smooth and low-density region with absorption resulting from neutral hydrogen instead of discrete clouds. This fluctuating photo-ionized gas in IGM suggests that the ordinary matter traces the distribution of underlying dark matter [5–8].

A part of this absorption in the Lyα forest is due to the UV transition of metals instead of neutral hydrogen. These metals are originated from enrichment by galactic winds. When column densities in some regions are larger than $\sim 10^{19}$ cm^{-2}., the outer regions of galaxies, Lorentzian wings dominate the absorption. These regions are called damped Lyman alpha (DLA) systems [9].

Hydrodynamical simulations have been effectively used to study the environments that cause Lyα forest [8,10–12]. In these environments, adiabatic cooling and photo-ionization heating in combination result in a strict relationship between temperature and gas density as $T \propto (\rho/\bar{\rho})^{\gamma-1}$ [13–15].

The relationship between the fraction of the transmitted flux and optical depth of the Lyα forest can be defined by $F = e^{-\tau}$. It can be shown that the power spectrum of transmitted flux $\delta F = (F/\bar{F}) - 1$ linearly traces the power spectrum of $\delta(x) = \rho(x)/\bar{\rho} - 1$ at large scale ($> 10h^{-1}Mpc$) [16]. However, at smaller scales, this relation is non-linear and more complex because of Jean's smoothing, thermal broadening, and nonlinear growth [17,18].

Initial studies [5,7,19–23] on Lyα forest clustering have focused on one-dimensional (1D) correlations along the line-of-sight toward a few quasars [24,25]. Larger data sets such as Sloan Digital Sky Survey (SDSS; [26]), Baryon Oscillation Spectroscopic Survey (BOSS; [27]), and extended Baryon Oscillation Spectroscopic Survey (eBOSS; [28]) were later used to repeat these 1D measurements.

In this article, the focus is on measuring the flux autocorrelation function in the Lyα forest. We use data from UVES[1] to measure the autocorrelation of the Lyα forest of 49 quasars.

The remainder of this paper is presented as follows. In the second section, the collection of high-resolution spectra is presented. In the third section, the solution to remove the polluting factors of the forest is explained. The calculation method for measuring the flux autocorrelation function is presented in the fourth section. In the fifth section, the obtained results are presented.

2 Quasar Dataset

In this section, the dataset used for measurement is introduced, and how to select parts of the selected data as Lyα forest is described.

The dataset comprises 49 spectra obtained using UVES on VLT [2], (Cerro Paranal, Chile). These 49 spectra were extracted from the ESO[3] archive. The VLT contains four individual telescopes, each armed with a primary mirror that measures 8.2 meters in diameter. These optical telescopes are usually used singly but can be combined to reach a very high angular resolution. The VLT array is also perfected by four transferable Auxiliary Telescopes (ATs) with 1.8-meter apertures. The VLT has the ability to observe both visible and infrared

[1]The Ultraviolet and Visual Echelle Spectrograph
[2]Very Large Telescope
[3]European Southern Observatory

wavelengths. Each telescope can detect objects that are almost four billion times weaker than what can be seen with the naked eye. When all the telescopes are merged together, they can reach an angular resolution of about 0.002 arcseconds. In a single telescope system, the angular resolution is about 0.05 arcseconds [29].

The QSO sample was chosen based on the following criteria:

(1) Complete or nearly complete coverage of the Lyα forest region;

(2) Mean signal-to-noise ratio greater than 20 in the Lyα forest region;

(3) Most spectra range from the atmospheric cutoff at $\lambda_{obs} \sim 3100$ to $\lambda_{obs} \sim 10000$Å.

Therefore, to search for metal lines, we can use a large range of spectrum to the red (longer wavelength) side of the Lyα forest. Figure 1 shows the distribution of (S/N) for the dataset used in the present work. The largest value of (S/N) is 120, and the smallest one is 21.

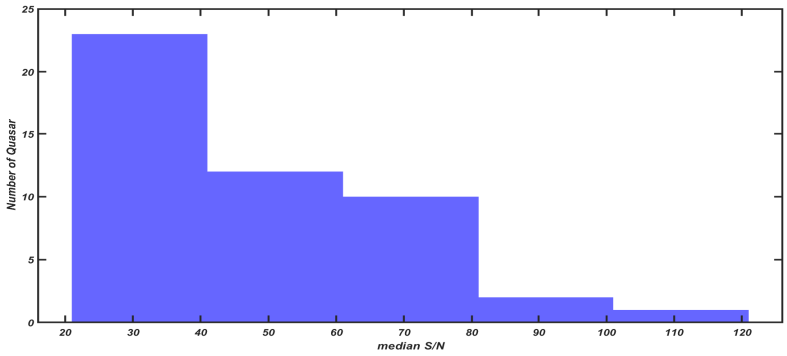

Figure 1: Histogram of the median (S/N) in the Lyα forest region used. Note that only spectra with $(S/N) > 20$ in the dataset are used.

In Table 1, the specifications of the used quasars' spectra are given. These specifications include the emission redshift, redshift range, and the wavelengths of Lyα forest covered by each spectrum. Moreover, in the third column of this table, the mean (S/N) per pixel in the Lyα forest zone between the emission lines of Lyα and Lyβ or O VI QSO is presented.

2.1 Determining Lyα forest region

The spectra were processed using the ESO data reduction package MIDAS[4] and the UVES pipeline interactively within a MIDAS context. For a comprehensive understanding of the pipeline, refer to the work of Ballester et al. [30]. After passing through the data reduction process, the raw data are usable in the form of three columns based on wavelength, flux, and noise.

To identify the wavelength region of the Lyα forest, it is necessary to determine the redshift of the quasar. Typically, the most prominent emission line of the quasar spectrum, the Lyα emission line is used to determine the redshift parameter, which is one of the defining parameters of a quasar. By fitting a Gaussian function to the highest peak of the

[4]The ESO-MIDAS system offers a range of tools for processing images and reducing data, focusing on astronomical uses such as imaging. It includes specialized reduction packages for ESO instruments at La Silla and the VLT at Paranal.

Table 1: QSOs sample in the present study. The columns give the QSO name, emission redshift (z_{em}), (S/N), redshift range covered by Lyα forest(z_{Ly_α}), and wavelengths covered by Lyα forest (λ_{Ly_α}), respectively.

Quasar name	z_{em}	(S/N)	z_{Ly_α}	λ_{Ly_α}	Note
J222756.90-224303.00	1.89	28.99	1.51–1.81	3047-3414	
J001602.39-001224.95	2.08	23.78	1.66–1.99	3239–3640	1DLA(z=1.97)
J133335.92+164903.94	2.09	33.63	1.66-1.99	3239-3640	1DLA(z=1.82)
he1341-1020	2.14	32.83	1.71-2.05	3299-3706	
J012417.43-374422.60	2.19	41.51	1.76-2.10	3356-3772	
J144653.17+011357.58	2.21	21.18	1.78–2.12	3375-3793	1DLA(z=2.08)
J103921.92-271918.34	2.23	79.48	1.78–2.12	3375-3793	
J024008.01-230916.70	2.24	77.48	1.78-2.13	3389-3808	
J145102.50-232930.01	2.25	48.49	1.78–2.13	3389–3801	
J000345.00-232355.00	2.26	48.78	1.82–2.17	3426–3850	
J110633.42-182124.05	2.32	24.56	1.86–2.22	3480–3911	
J011143.60-350300.68	2.40	62.23	1.94–2.30	3573–4015	
J112442.84-170516.76	2.41	120.24	1.94-2.30	3574-4015	
he2217-2818	2.41	39.41	1.95-2.31	3585-4027	
J222006.70-280321.28	2.42	75.88	1.95–2.31	3586–4030	
J033106.43-382404.97	2.44	40.73	1.97–2.34	3614–4062	
J120044.98-185942.79	2.45	48.11	1.97–2.34	3617–4065	
J004201.21-403038.52	2.48	25.36	2.00–2.38	3652–4105	
J220852.13-194359.20	2.57	44.91	2.08–2.46	3748–4212	
J123437.60+075846.13	2.58	29.98	2.08–2.46	3746–4210	1DLA(z=2.33)
J135038.96-251215.84	2.62	49.30	2.12-2.51	3794-4264	
J114254.47+265500.80	2.63	68.01	2.13-2.51	3800-4269	
J045523.09-421618.70	2.66	58.79	2.15–2.54	3834–4309	
J000852.65-290041.69	2.67	29.28	2.16–2.55	3839–4315	1DLA(z=2.53)
J033244.06-445556.42	2.67	26.83	2.17–2.56	3855–4333	1DLA(z=2.42)
J033108.98-252442.91	2.70	29.67	2.20–2.59	3886–4367	
q000-422	2.76	40.31	2.25–2.65	3951–4441	
J091614.05+070225.19	2.78	52.51	2.26–2.67	3970–4462	1DLA(z=2.62)
he0151-4326	2.78	70.29	2.62–2.63	3967–4458	
J141217.41+091624.28	2.84	55.18	2.32–2.73	4043–4535	2DLA(z=2.46,2.67)
he2347-4342	2.87	47.63	2.34-2.75	4063–4566	
J021857.24+081729.18	2.99	23.78	2.45–2.72	4194–4521	
J040718.04-441013.87	3.00	31.92	2.46–2.89	4205–4725	1DLA(z=2.57)
J135647.04-110127.08	3.00	23.76	2.45–2.88	4199–4718	1DLA(z=2.50)
J194025.86-690757.47	3.18	40.89	2.93–3.06	4779–4934	
J134259.00-135600.60	3.21	35.17	2.63–3.78	4413-4959	
J034943.55-381030.76	3.22	27.81	2.65–3.10	4433–4982	1DLA(z=3.02)
J212912.12-153838.54	3.27	90.53	2.69–3.15	4492–5048	
J121134.92+090221.48	3.29	31.10	2.70–3.16	4499–5056	
J111350.64-153332.04	3.36	27.31	2.77–3.23	4580–5147	1DLA(z=3.24)
J010604.30-254653.40	3.37	20.84	2.77–3.24	4589–5157	
J115538.61+053049.72	3.47	43.83	2.85–3.33	4688–5268	1DLA(z=3.33)
J123055.71-113908.21	3.54	31.65	2.93–3.40	4779–5325	
J005758.14-264315.49	3.64	27.31	3.01–3.51	4878–5482	
J124957.54-015927.60	3.68	42.10	3.03–3.53	4903–5510	
J132029.97-052334.51	3.71	38.21	3.07–3.57	4950–5563	
J162116.91-004249.79	3.72	47.56	3.06–3.56	4934–5545	1DLA(z=3.11)
J200323.99-325144.35	3.78	65.46	3.13–3.64	5023–5644	1DLA(z=3.18)
J193957.23-100241.14	3.80	67.99	3.14-3.66	5037-5661	

quasar spectrum or through observational methods, the wavelength of Lyα emission can be obtained. After finding the Lyα emission line, the redshift parameter z is defined as Equation1, where λ_0 represents the rest-frame wavelength of a spectral line and λ_{obs} is the observed wavelength

$$z_{em} = \frac{\lambda_{obs} - \lambda_0}{\lambda_0}. \quad (1)$$

Only the rest-frame wavelengths in the range 1050 Å$< \lambda <$1180 Åare used to prepare the autocorrelation function data. In this way, the Lyα proximity region ([31–35]), which possibly corresponds to large redshift errors, is excluded. Moreover, this excludes the emission lines of Lyβ and OVI λ=1035Åas well as their possible blueshifted absorption besides errors of continuum fitting near the emission lines. This range is also used as a conservatively chosen Lyα forest region [27,36,37].

The main purpose of studying the autocorrelation function is to analyze the structure and distribution of the baryonic matter distribution in the universe, especially in the case of neutral hydrogen gases of Lyα forest. In this context, obtaining the QSO continuum is very important as it allows us to accurately interpret the absorption features in the Lyα forest and subsequently derive the matter distribution. Accordingly, we must initially obtain the QSO continuum in the Lyα forest.

The Smooth Local (SL) method is used to fit the continuum of a spectrum to the Lyα forest regions that are "free of absorption lines" based on visual assessment. To do this, unabsorbed regions in the forest have to be identified and then connected using smoothing splines. The top panel of Figure 2 shows the results of the SL method for one QSO in the Lyα forest region. This method can be used for the estimation of the continuum in the Lyα forest without requiring a wide wavelength range in the red side of the Lyα emissions [38].

In the following, having a continuum, the spectrum of each quasar is normalized. To obtain the normalized spectrum, the ratio of the observed spectrum to estimating the continuum spectrum was obtained. In the bottom panel of Figure 2, the normalized spectrum of the Lyα forest segment corresponding to one of the sample quasars can be seen [39].

3 Cleaning up Lyα forest

Metal absorption changes the transmitted fraction in the QSO spectrum. Therefore, the autocorrelation function can also be changed [25]. This implies that the autocorrelation function can be used to determine statistical characteristics of the Lyα forest by removing the metal absorption from the Lyα forest in the QSO spectrum.

To reduce the contamination of high column density absorbers, parts of the spectrum (e.g., DLAs) and metal lines were masked. When a pixel was already masked in the reduction process (for example by cosmic ray or spectral gap), it remained masked.

Although, absorbers with clear visible damping wings (DLAs) have existed. the results of this study were certainly not affected by these absorbers. This was done by masking the wings and core of these strong absorbers based on visual inspection. This technique mainly excludes big continuous spectral areas. Consequently, a spectrum with DLAs is only shorter in length, but there are no extra gaps in the data.

The effects of metal absorption in our spectra were reduced by masking metal lines in the forest region. Initially, DLAs within the forest were found, and all strong metal absorption lines related to DLA redshifts were masked. This was carried out using the metal transition details in Table 2 and masking by a radius of 60 (km/s) around each of the absorbers.

Subsequently, we searched for absorption from common doublet transitions (Si IV, NV, C IV, Mg II, Al III, and Fe II) redward of the forest where the spectrum is mostly clean.

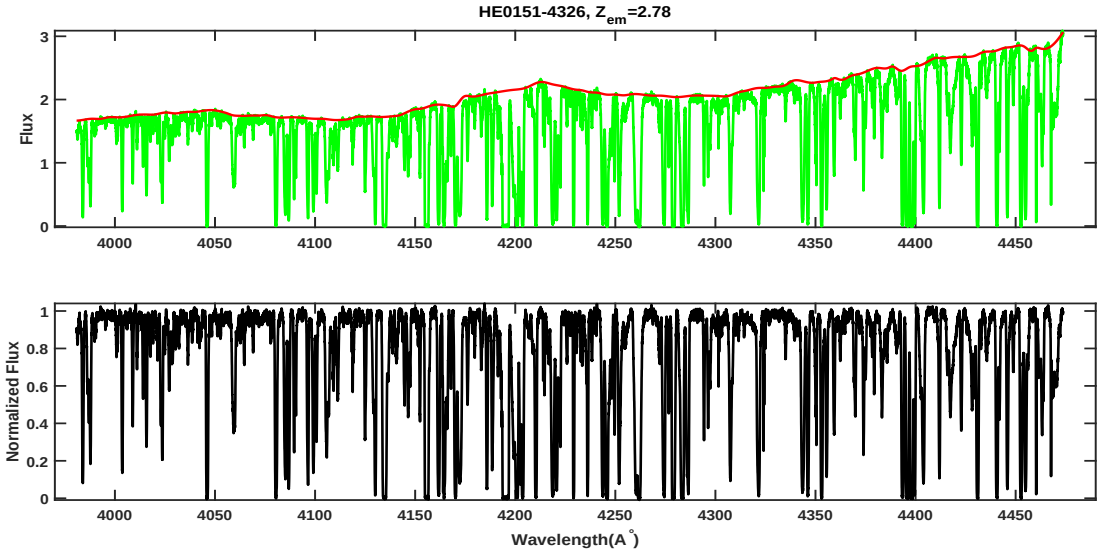

Figure 2: In the top panel: SL continuum fitting results for one QSO. The red line represents the continuum spectrum, and the green pattern is the HE0151-4326 spectrum at redshift $z_{em} = 2.78$ in the Lyα forest region. In the bottom panel: the normalized flux (the ratio of the observed spectrum to the estimated continuum spectrum).

Then, we masked the corresponding metal lines similar to our technique for DLAs (with the same mask width and metal catalog), such that no doublet feature remained redwards of the forest.

An example is shown in Figure 3 to indicate the extent of masking in a typical spectrum. The dark green color represents the non-masked part of the spectrum, and the red color represents the parts that were masked due to possible metal contamination.

These methods never produce a completely metal-free Lyα forest, and we briefly address their limitations. Searching for metals in the red side of the Lyα forest yields meaningful results only when both binary counterparts are observable at wavelengths longer than the Lyα emission line. If a binary counterpart falls into a spectral range that is not covered or overlaps with another line (from a different redshift), the contaminated system is often undetected. On the other hand, particularly for higher redshift, a significant portion of the spectral range towards the forest red is affected by telluric absorption, complicating the detection of binaries. Therefore, the primary challenge of this method is the limited usable spectral coverage in the red region.

Figure 4 gives an overview of the dataset. In this figure, the full coverage for each quasar spectrum is illustrated after masking DLAs, metal lines, and pre-existing gaps in the data. The remaining spectrum can be categorized as the used data (darker color) and masked data(DLAs and metal lines) resulting from possible contaminations and pre-existing gaps (lighter color).

Table 2: List of metal transitions that were masked.

Ion	λ_{rest}	Ion	λ_{rest}
O VI	1031.936	Si IV	1402.770
C II	1036.337	Si II	1526.707
O VI	1037.617	C IV	1548.195
N II	1083.990	C IV	1550.770
Fe III	1122.526	Fe II	1608.451
Fe II	1144.938	AL II	1670.787
Si II	1190.416	AL III	1854.716
Si II	1193.290	AL III	1862.790
N I	1200.710	Fe II	2344.214
Si III	1206.500	Fe II	2374.461
N V	1238.821	Fe II	2382.765
N V	1242.804	Fe II	2586.650
Si II	1260.422	Fe II	2600.173
O I	1302.169	Mg II	2796.352
Si II	1304.370	Mg II	2803.531
C II	1334.532	Mg I	2852.964
C II	1335.708	Ca I	3934.777
Si IV	1393.755	Ca I	3969.591

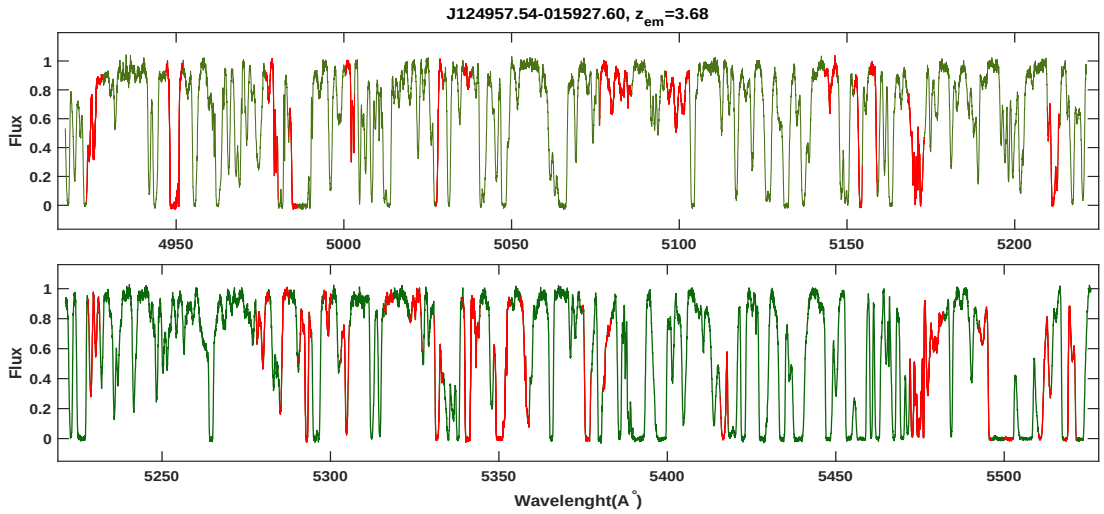

Figure 3: The Lyα forest region for one of our spectra (J124957.54-015927.60) with regions masked because of possible metal contaminations (in red). The dark green color represents the non-masked parts. Note that our approach masks not only metals but also coincidental pieces of the Lyα forest.

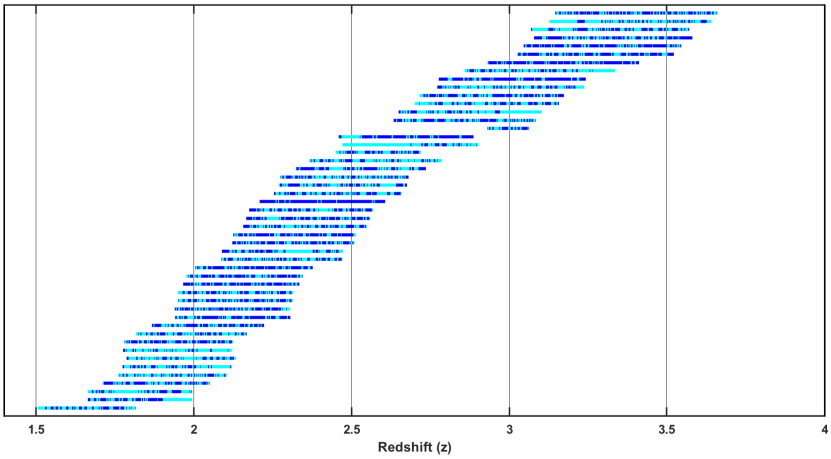

Figure 4: Redshift coverage of the employed dataset. The spectral coverages of used spectra for the UVES in the Lyα forest are shown by blue lines. but segments in lighter color denote masks resulting from possible metal and DLAs contaminations

4 Autocorrelation function

One of the important fields in cosmology is the investigation of clustered structures, which can provide valuable information about cosmological models, as well as the constituents of the universe and their evolution [41]. The flux autocorrelation function, denoted by ξF(v), is a statistic that can be easily calculated. Zuo & Bond (1994) [21] and Cen et al (1998) [42] highlighted the benefits of using this function. Calculating the Autocorrelation function is another way to statistically analyze the Lyα forest without the need to count lines, using the intensity of pixels. Additionally, if the continuum is considered uniformly by a higher or lower constant factor, the Autocorrelation function remains unaffected. Considering such characteristics, it becomes a powerful tool for extracting information from the Lyα forest in high-quality data explosions captured by 10m-class telescopes. In this section, we explain our measurement of the autocorrelation function using the details in Table 1.

The measurement of $\xi F(v)$ can be performed in the radial direction independent from each QSO spectrum. We estimate $\xi F(v)$ from our quasar data in Table 1 using the estimator $\xi F(v) = \delta F(x)\delta F(x+v)$ [43]. Next, the autocorrelation function is calculated in terms of speed, which is obtained from the observed wavelength as follows:

$$\frac{\Delta\lambda}{\lambda} = \frac{\Delta v}{c}, \tag{2}$$

where c is the speed of light, $\Delta\lambda$ is the wavelength change, and Δv is the speed difference. The flux autocorrelation function can be calculated for the observational data of the spectrum of quasars using equation 3. In this equation, F is the normalized flux, $< F >$ is the mean flux for all pixels, v is the line-of-sight velocity, and $\Delta\ v$ is the radial velocity step. To compare the autocorrelation functions, they are normalized using equation 4. Figure 5 shows the results of the flux autocorrelation functions in the Lyα forest for some examples of quasars:

$$\xi(\Delta v) = \left\langle \left(\frac{F_v}{\langle\ F\rangle} - 1 \right) \left(\frac{F_{\Delta v+v}}{\langle\ F\rangle} - 1 \right) \right\rangle, \tag{3}$$

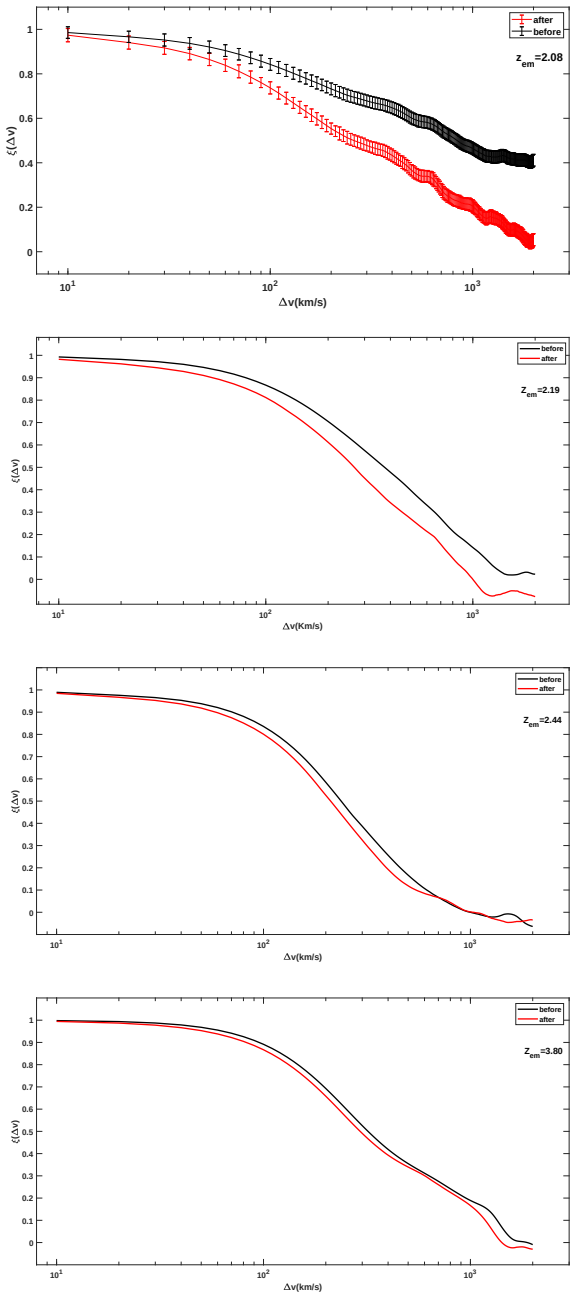

Figure 5: Flux autocorrelation functions in the Lyα forest for quasars with redshifts ($z_{em} = 2.08, 2.19, 2.44,$ and 3.80. The black graphs are related to the functions before the removal of contamination and the red graphs are related to the results after the removal of contamination. In the case of $z_{em} = 2.08$, the error bar measured by the bootstrap method can be seen.

$$\xi(\Delta v) = \frac{\left\langle \left(\frac{F_v}{\langle F \rangle} - 1\right)\left(\frac{F_{\Delta v+v}}{\langle F \rangle} - 1\right)\right\rangle}{\langle F \rangle^2}. \quad (4)$$

These equations are used for each quasar sample before and after clearing the Lyα forest. The flux autocorrelation functions are drawn for four sample quasars in the lowest and highest redshifts in Table 1 (z_{em} = 2.08, 2.19, 2.44, and 3.80). As can be seen (Figure 5), the removal of metal lines affects the curve of the flux autocorrelation function. In order to

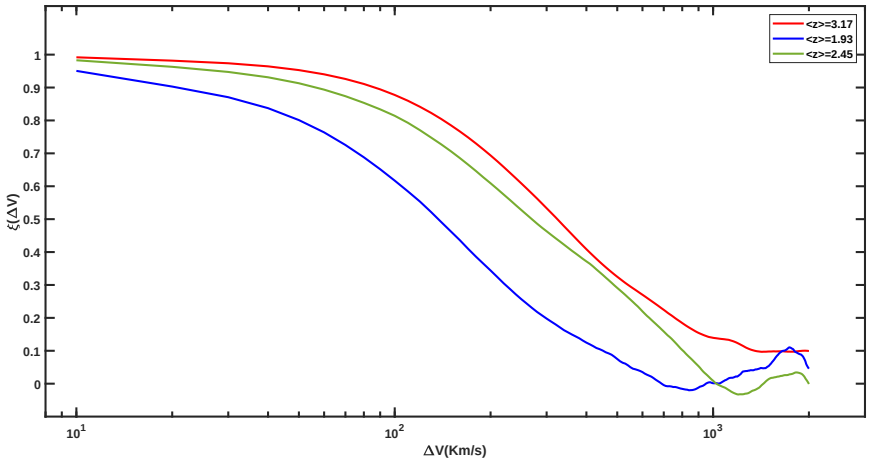

Figure 6: Flux autocorrelation functions for the spectrum of three quasars with average redshifts $< z >$=3.17 in red, $< z >$=2.45 in green, and $< z >$=1.93 in blue.

have a better attitude towards the autocorrelation function of Lyα forest and to investigate the effect of redshift on it, after drawing all the autocorrelation functions for 49 spectra, three of them with average redshift $< z >$=3.17, $< z >$=2.45, and $< z >$=1.93. have been selected and compared. Figure 6 shows the effect of redshift on the flux autocorrelation function.

5 Results

In this study, the flux autocorrelation function was measured for 49 quasars in the emission redshift range of 2.08$< z_{em} <$3.80 with high resolution and signal-to-noise ratios larger than 20. Low spectral resolution can lead to the loss of important information about absorption lines. The low resolution is not sufficient for data analysis, making it difficult to identify the exact features of the absorption lines. In this work, an attempt was made to use spectra with high resolution, but the need for high-quality spectra is still felt. Data with a low signal-to-noise ratio can lead to significant errors in absorption measurements and autocorrelation function analysis. This problem is especially evident in low-resolution studies. The most important challenge to determine the autocorrelation function was determining the continuum and accurate determination of metal lines. Having spectra with high signal-to-noise makes these challenges easier. These findings can be compared to the predictions of any cosmological simulation consistent with a particular theory when instrumental resolution and noise comparable to our data are included in the simulated spectra. Furthermore, any

subsequent observational assessment of these same measures from alternative datasets also allows direct comparison. The results of this study can be summarized as follows:

1. The comparison of two flux autocorrelation functions before and after the removal of contamination for each quasar (Figure 5) indicates that the effect of removal is more visible in transition to lower redshifts, where there are relatively fewer Lyα absorption lines.
2. The flux autocorrelation function generally shows lower values for all quasars after removing contaminations (see Figure 5 as an example).
3. For the transition to lower redshifts, where the effect of contamination is more visible, the drop in flux autocorrelation function is stronger.
4. The flux autocorrelation function in transition to higher redshifts has a higher average value than that in transition to lower redshifts (see Figure 6).

The results obtained in this study can be compared with the work of McDonald et al (2000) [25]. MacDonald et al used a sample of eight quasars observed at high resolution and signal-to-noise ratio to determine the correlation function. However, their approach to removing metal lines differs from the methodology employed in this study. A key difference lies in the fact that McDonald et al. utilized simulated spectra of the Lyα forest in their analysis, whereas this research relies on observational data. The result of this research can be used to calculate the power spectrum and investigate the fluctuations of baryons in the universe. In order to achieve the goal of investigating the IGM, the results can be used to validate new theories, and determine cosmological parameters.

Authors' Contributions

All authors have the same contribution.

Data Availability

The data that support the findings of this study are available from the corresponding author upon reasonable request.

Conflicts of Interest

The authors declare no potential conflicts of interest.

Ethical Considerations

The authors have diligently addressed ethical concerns, such as informed consent, plagiarism, data fabrication, misconduct, falsification, double publication, redundancy, submission, and other related matters.

Funding

This research did not receive any grant from funding agencies in the public, commercial, or nonprofit sectors.

References

[1] Nicolson, I. 1999, Unfolding our univer, Cambridge univ. press, Cambridge.

[2] Gunn, J. E. & Peterson B. A. 1965, ApJ, 142, 1633.

[3] Bahcall, J. N. & Salpeter, E. E. 1965, ApJ, 142, 1677.

[4] Lynds, R. 1971, ApJ, 164, 73.

[5] Cen, R., Miralda-Escude′, J., & Ostriker, J. P. 1994, ApJ, 437, 9.

[6] Zhang, Y., Anninos, P., & Norman, M. L. 1995, ApJ, 453, 57.

[7] Hernquist, L., Katz, N., Weinberg, D. H., Jordi, M. 1996, ApJ, 457, 51.

[8] Theuns, T., Leonard, A., Efstathiou, G., Pearce, F. R., & Thomas, P. A. 1998, MNRAS, 301, 478.

[9] Mo, H. 2010, Galaxy formation and evolution, Cambridge Univ. Press, cambridge.

[10] Miralda-Escud′e, J., Cen, R., Ostriker, J. P., & Rauch, M. 1996, ApJ, 471, 582.

[11] Wadsley, J. W. & Bond, J. R. 1997, in Astronomical Society of the Pacific Conference Series, Vol. 123, Computational Astrophysics; 12th Kingston Meeting on Theoretical Astrophysics, ed. D. A. Clarke , M. J. West, 332.

[12] Zhang, Y., Anninos, P., Norman, M. L., Meiksin, A. 1997, ApJ, 485, 496.

[13] Hui, L., Gnedin, N. Y. 1997, MNRAS, 292.

[14] Puchwein, E., Bolton, J. S., Haehnelt, M. G., et al. 2015, MNRAS, 450, 4081.

[15] McQuinn, M., Upton Sanderbeck, P. R. 2016, MNRAS, 456, 47.

[16] Slosar, A., Font-Ribera, A., Pieri, M.M., Rich, J., Goff, M. L., Aubourg, E. et al. 2011, JCAP, 001.

[17] McDonald, P. 2003, ApJ, 585, 34.

[18] Givans, J. J., Font-Ribera, A., Slosar, A., & Seeyave, L. 2022, JCAP, 070.

[19] Rauch, M., Miralda-Escude′, J., Sargent, W. L. W., Barlow, T. A., et al. 1997, ApJ, 489, 7.

[20] Zuo, L. 1992, MNRAS, 258, 36.

[21] Zuo, L. & Bond, J. R. 1994, ApJ, 423, 73.

[22] Hui, L. 1999, ApJ, 516, 519.

[23] Cen, R., Phelps, S., Miralda-Escude′, J., & Ostriker, J. P. 1998, ApJ, 496, 577.

[24] Croft, R. A. C., Weinberg, D. H., Katz, N., & Hernquist, L. 1998, ApJ, 495, 44.

[25] McDonald, P., Miralda-Escud′e, J., Rauch, M., Sargent, W. L. W., Barlow, T. A., R. Cen, R., et al. 2000, AJ, 543.

[26] McDonald, P., Seljak, U., Burles, S., Schlegel, D. J., Weinberg, D. H., Cen, R. et al. 2006, ApJS, 163.

[27] Palanque-Delabrouille, N., Y'eche, C., Borde, A., Goff, J.-M.L., Rossi, G., Viel, M., et al. 2013, A&A, 559, A85.

[28] Chabanier, S., Palanque-Delabrouille, N., Y'eche, C., Goff, J.-M.L., Armengaud, E., Bautista, J., et al. 2019, JCAP,017.

[29] European Southern Observatory (ESO), http://www.eso.org/public.

[30] Ballester, P., Modigliani, A., Boitquin, O., Cristiani, S., Hanuschik, R., Kaufer,A., & Wolf, S. 2000, in The Messenger, 101, 31.

[31] Bechtold, J. 1994, ApJS, 91, 1.

[32] Srianand, R. & Khare, P. 1996, MNRAS, 280, 767.

[33] Liske, J. & Williger, G. M. 2001, MNRAS, 328, 653.

[34] Prochaska, J. X., Hennawi, J. F., Lee, K.-G., et al. 2013, ApJ, 776, 136.

[35] Khrykin, I. S., Hennawi, J. F., McQuinn, M., & Worseck, G. 2016, ApJ, 824, 133.

[36] Priyanka, J., Hum, Ch., & Srianand, R. 2019, APJ, 884, 151.

[37] Walther, M., Hennawi, J., Hiss, H., O′norbe, J., Lee, Kh. G., Rorai, A., & O'Meara, J. 2018, APJ, 852 ,22.

[38] Aghaee, A., Petitjean P., Srianand,R., Stalin, C. S., & Guimar′aes, R., 2010, J. Astrophys. Astron., 31, 59.

[39] Calura, F., Tescari, E., D'Odorico, V., Viel, M., Cristiani, S., & Kim, T.-S., Bolton J.S., 2012, MNRAS,422, 3019.

[40] Croft, R. A., Weinberg, D. H., Pettini, M., Hernquist, L., & Katz,N. 1999, ApJ, 520, 1.

[41] Andrew, R. M., Kristoffer, A. E., Chris, D. I., & Lei, B. 2008, ApJS, 175, 29.

[42] Cen, R. & Ostriker, j. P. 1999, ApJ, 514 ,1.

[43] Becker, G.D. & Rauch, M. 2004, ApJ, 613, 61.